Suppression of Deflecting Forces in Planar-Symmetric Dielectric Wakefield Accelerating Structures with Elliptical Bunches

Brendan D. O'Shea, Gerard Andonian, S. S. Baturin, Christine I. Clarke, P. D. Hoang, Mark J. Hogan, Brian Naranjo, Oliver B. Williams, Vitaly Yakimenko, and James B. Rosenzweig

Phys. Rev. Lett. **124**, 104801 — Published 11 March 2020

DOI: 10.1103/PhysRevLett.124.104801

Suppression of Deflecting Forces in Planar-Symmetric Dielectric Wakefield Accelerating Structures with Elliptical Bunches

Brendan D. O'Shea,[1,2,*] Gerard Andonian,[1] S. S. Baturin,[3] Christine I. Clarke,[2] P. D. Hoang,[1] Mark J. Hogan,[2] Brian Naranjo,[1] Oliver B. Williams,[1] Vitaly Yakimenko,[2] and James B. Rosenzweig[1]

[1]*Department of Physics and Astronomy, University of California, Los Angeles, California 90095, USA*
[2]*SLAC National Accelerator Laboratory, Menlo Park, California 94025, USA*
[3]*Department of Electrical Engineering and Department of Physics, Northern Illinois University, DeKalb, IL 60115*

(Dated: December 16, 2019)

Wakefield based accelerators capable of accelerating gradients two orders of magnitude higher than present accelerators offer a path to compact high energy physics instruments and light sources. However, for high gradient accelerators, beam instabilities driven by commensurately high transverse wakefields limit beam quality. It has been previously theoretically shown that transverse wakefields can be reduced by elliptically shaping the transverse sizes of beams in dielectric structures with planar symmetry. We report here experimental measurements that demonstrate reduced transverse wakefields for elliptical beams in planar symmetric structures which are consistent with theoretical models. These results may enable the design of gigavolt-per-meter gradient wakefield based accelerators that produce and stably accelerate high quality beams.

Next-generation acceleration schemes based on electomagnetic wakefields driven in dielectric-lined structures, known as dielectric wakefield accelerators (DWA), have recently demonstrated GeV/m accelerating gradients [1]. In DWAs, an intense drive beam generates a wakefield that is used to accelerate an appropriately phased trailing beam, or witness beam. With large amplitude wakefields, the trailing beam can attain very high energy in short distances; this is an advantageous development that may yield compact high-energy accelerators for future colliders and X-ray light sources. However, these high accelerating gradients are accompanied by commensurately high transverse wakefields that may negatively affect beam stability and quality [2]. This situation arises in large part due to the need for using small-scale, high frequency structures to obtain high wakefield coupling. Demonstrating effective strategies for mitigating transverse wakefields is thus a critical step towards developing efficient, high gradient wakefield accelerators.

A transverse wakefield-driven instability is generated when a beam travels off-axis through an accelerating structure [3], giving rise to fields having net transverse forces that cause the beam to undergo unstable motion, ultimately degrading beam quality. These fields increase as the accelerating gradient is increased, and so their effects must be ameliorated. Thus, the requirement of preserving the quality of the beam during acceleration requires a trade-off between accelerating gradient and beam quality [4]. Several methods have been developed to mitigate the effects of transverse forces on beam quality. For example, in radio-frequency accelerators the transverse quality of the beam is preserved using a combination of alternating gradient focusing and longitudinally correlated energy spread that decouples the motion of longitudinal slices of the beam, an approach termed Balakin-Novokatsky-Smirnov (BNS) damping [4–7]. Alternative methods to suppress transverse forces appropriate for wakefield accelerators involve the direct reduction of the coupling of the beam to transverse modes by manipulating the beam shape in structures with specific geometrical properties. Indeed, the method studied in this Letter employs beams with highly elliptical aspect ratio in a DWA having a planar geometry to inhibit coupling to modes and generation of transverse forces. While this scheme was proposed over two decades ago [8], it has only been recently possible to experimentally explore its efficacy in a high gradient DWA environment, as reported here.

The use of elliptical beams in planar DWA structures as a method of suppressing transverse forces has been investigated analytically by direct solution to Maxwell's equations with appropriate boundary conditions [8], in detailed simulations [9, 10], and using conformal mapping of Green's function solutions [11]. In previous experimental work, DWAs in planar geometries have been studied in the context of acceleration at moderate energy [12, 13], and spectral decomposition in woodpile [14] and Bragg-reflector [15] configurations. However, the low charge density and resultant gradients present in these experiments prevented the observation of transverse effects to appreciably measurable levels. Here, we present first measurements of the reduction of transverse forces in planar DWA structures at high energy and high gradients, with intense drive beams through the variation of the beam's transverse ellipticity.

The physical mechanism underlying this transverse wakefield suppression is the reduction of the coupling of the beam to structure modes that produce net transverse forces on the beam. For slab symmetric structures, the coupling term is a function of the scaled beam width parameter, $\chi \equiv \sigma_y/a$, where a is the half width of the vacuum gap of the dielectric-lined structure and σ_y is the r.m.s. beam size perpendicular to that vacuum gap (*c.f.* Figure 1). Point-like beams, $\chi = 0$, will couple

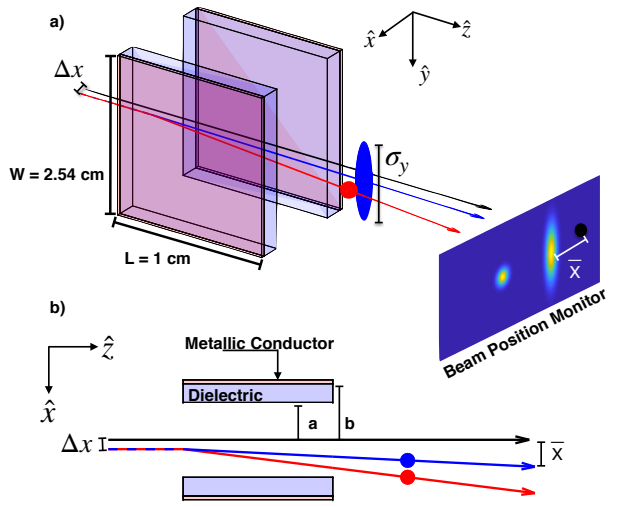

FIG. 1. a) Isometric and b) top-down view of the layout of the experiment. Beams propagate from left to right, in the $\hat{z}$ direction. An initial displacement in the structure, Δx, is added by moving the structure perpendicular to the direction of beam propagation, along the $\hat{x}$ direction. The average offset of the beam in the $\hat{x}$ direction, $\bar{x}$, is measured 6.64 m downstream of the structure using a beam position monitor (BPM). The black dot indicates the undisturbed beam propagation direction, when the beam is on-axis in the structure.

to all modes supported by the structure, which results in maximum longitudinal (acceleration) as well as transverse forces. Conversely, beams that are large compared to the vacuum gap (*i.e.* asymmetric beams with large aspect ratios), $\chi > 1$, will couple less effectively to the structure modes [11]. Theoretical work shows that coupling to the transverse modes falls off faster than the coupling to the longitudinal modes, $1/\chi^3$ compared to $1/\chi$ [8][11]. This scaling can be exploited to reduce the effects of transverse wakefields in high gradient, high frequency accelerators with planar symmetry. Furthermore, the theoretical work shows that the coupling is purely geometry dependent and not dependent on specific dielectric material.

In this Letter we present parametric studies on the effects of beam ellipticity and dielectric material on transverse wakefields in a planar DWA. The effects of transverse wakefields over the length of the structure are measured as an integrated transverse kick experienced by the beam, as quantified by the centroid displacement from the nominal unperturbed trajectory (Figure 1). These data demonstrate the feasibility of using transverse bunch shaping to suppress transverse wakefields and confirms that the effect is geometric, and not dependent on the dielectric material. Simulations and analytic models of transverse wakefield induced integrated kick are shown to agree with the measured data.

The experiments presented in this work were conducted at the Facility for Advanced aCcelerator Experimental Tests (FACET) at the SLAC National Accelerator Laboratory [16]. A two-km linac provides 20.35 GeV beams consisting of $N_e = 2 \times 10^{10}$ electrons with a root mean square (r.m.s.) bunch length of $\sigma_z = 30$ μm [17]. A diagram of the experiment is shown in Fig. 1. A magnetic optics focusing system consisting of two quadrupole triplets is used to deliver electron beams in the interaction region with with fixed r.m.s. transverse beam size $\sigma_x = 90$ μm and σ_y adjustable from 90 to 450 μm. More details on the electron beam optics can be found in Ref. [18]. Beam sizes are measured using optical transition radiation images. Additionally, a bench-marking experiment was performed in an annular DWA structure using nearly round beams with transverse beam size $\sigma_x = 40$ μm, $\sigma_y = 52$ μm, $\sigma_z = 40$ μm and $N_e = 0.7 \times 10^{10}$ electrons. The baseline experiments operate at reduced charge to mitigate high-field effects uncovered in previous DWA experiments [19], and allow the precision measurement of mode frequencies excited in the structure.

Due to the relatively short interaction length and other experimental constraints, simultaneous measurement of both transverse wakefields and accelerating gradients was not possible. However, theoretical calculations, using the same methods described below for determining the transverse forces, show that the peak accelerating gradient in these experiments varies from 320 MeV/m for the widest beams to 584 MeV/m for the narrowest. These gradients are close to the desired goals for future accelerators. Measurement of stable acceleration using 1000 MeV/m accelerating gradients are planned at the forthcoming FACET-II facility. The remainder of this Letter concentrates on the measurement and mitigation of transverse wakefields required for stable beam transport at such high accelerating gradients.

Normalized beam size ratios, $\chi \equiv \sigma_y/a$, in the range $\chi = 0.375$-2.35 were used, where $a = 240$ μm is the half width of the vertical vacuum gap of the DWA, *c.f.* Figure 1. The DWA structures are positioned with respect to the beam by a 5-axis motor system with approximately μm precision, and assisted by an alignment laser that is matched to the electron beam trajectory [1]. For each normalized beam size χ the initial displacement Δx of the beam with respect to the DWA symmetry axis was scanned from -100 μm to 100 μm in steps of 20 μm. The deflection of the centroid of the beam, $\bar{x}$, on a beam position monitor (BPM) Δz=6.64 m downstream of the structure was used to quantify the integrated transverse kick received by the beam as a function of initial displacement in x inside of the DWA.

In addition to direct observation of beam deflection using a BPM, the spectral content of the wakefields in the cylindrical structure reveals the excitation of transverse modes when the beam is not aligned to the symmetry plane of the DWA. The frequency spectrum confirms that the effect under investigation is directly related to the transverse forces excited by off-axis beam passage

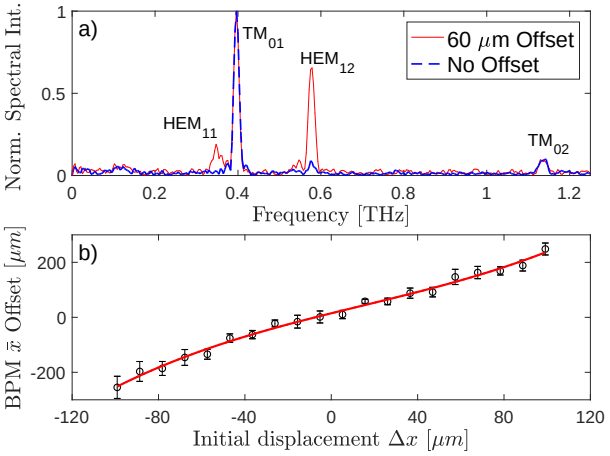

FIG. 2. a) Spectral content of an annular DWA when an electron beam travels down the symmetry axis (blue, dashed) and 60 μm offset from the symmetry axis (red). When traveling off-axis, the electron beam couples to hybrid electromagnetic (HEM) modes that result in transverse forces on the beam. b) The measured average offset of the beam on the BPM, $\bar{x}$, as a function of the initial displacement in the structure, Δx is shown. The red line represents a fit to the data and is used to calculate the strength of the linear forces on the beam.

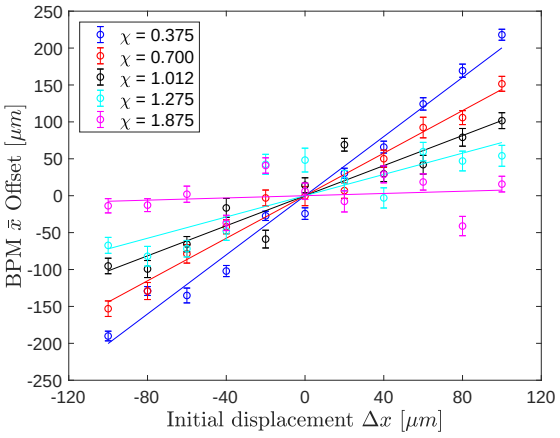

FIG. 3. The measured average final offset of the beam as observed downstream of the planar structures, $\bar{x}$, as a function of Δx. The colors represent different beam sizes normalized the to vacuum half gap, $\chi = \sigma_y/a$. For each value of χ a linear fit is performed and used to calculate the integrated transverse forces on the beam.

through the structure. The spectra were obtained using a Michelson interferometer [1, 19]. A set of off-axis parabolic mirrors are used to collect and image the beam exit point from the DWA to the interferometer. The system is designed such that the radiation emitted from the structure is preferentially directed 30° away from the beam axis. This Vlasov-type antenna [20, 21] improves the signal to noise ratio in the interferometer by reducing the collection of axially directed (*i.e.* transition radiation) beam-derived coherent emissions. A fast-Fourier transform of the autocorrelation generated by scanning the interferometer delay is performed to generate the modal content of the wakefields excited in the DWA. For each set of measurements in this work the spectra are normalized to those obtained for round, on-axis beams.

To demonstrate the dependence of transverse forces on system geometry, three dielectric wakefield accelerators were used in these experiments, two with planar symmetry, and one with, as noted above, an annular geometry. The parameters of each DWA structure are outlined in Table I. All DWAs were of length L=1 cm. The width in x of the planar structures is W=2.54 cm, which satisfies the condition that the structure width be much wider than the beam dimensions in all cases [11], $\sigma_{x,y}/W \ll 1$. The slabs are cut to size from bulk wafers using a diamond saw and are held in place by precisely machined aluminum holders that also form the metallic walls of the DWA. The fabrication process for the annular structures has been described in previous work [1].

Figure 2a shows the spectral content of the wakefields collected for the annular DWA. As expected, in the annular structure there is no excitation of the undesired transverse (HEM) modes when the beam is on axis (blue, dashed line). However, transverse modes (HEM_{11} and HEM_{12}) are evident when the beam is displaced off-axis by 60 μm (red line). Figure 2b shows the average offset of the beam $\bar{x}$ measured by the downstream BPM, as a function of the beam's initial displacement inside the structure, Δx. The offset is fit to a model that incorporates both the dipole (linear) and higher order transverse (cubic) terms [3, 22] as $\bar{x}(\Delta x) = a + b(\Delta x - c) + d(\Delta x - c)^3$, where the coefficients b and d represent the contributions of the dipole and higher-order mode terms, respectively. The model fit is shown in Fig. 2b in red, and has a linear slope of $b = 1.91 \pm 0.25 \mu\text{m}/\mu\text{m}$. From this slope the average transverse force per μm offset is calculated to be $\bar{F}_x = \frac{\gamma mc^2}{\Delta z L} b = 0.57 \pm 0.08 \frac{MeV}{m \cdot \mu m}$. Throughout this work the quoted errors represent the 95% confidence interval. As planar structures generate smaller wakefields in general, and higher order mode excitation also decreases as χ increases, the cubic component cannot be resolved in the planar structure measurements. For the planar structure measurements d is not considered in the fitting model.

The DWA length is small compared to the distance between the structure exit and the diagnostic BPM, $L \ll \Delta z$, so the calculation of the integrated transverse force has a weak dependence on the component of $\bar{x}$ achieved inside the structure. 3D simulations using VORPAL [23] support this assumption and further show that transient effects from the entrance and exit of the structure account for $\leq 10\%$ of the kick for a given offset. This effect is captured by the larger error bars in the measured offset $\bar{x}$ for larger initial displacements, *c.f.* Fig. 2b.

This procedure is also performed for the planar struc-

Structure	$\chi = \sigma_y/a$	$\bar{F}_x$ $[\frac{MeV}{m\cdot\mu m}]$ Measured	Theory
Annular SiO_2	0.260	0.587	0.546
Slab SiO_2	0.375	0.614	0.627
a = 240 μm	0.700	0.442	0.402
b = 450 μm	1.013	0.312	0.254
$\epsilon = 3.8$	1.275	0.220	0.175
	1.875	0.023	0.085
Slab ZTA	0.350	0.514	0.566
a = 240 μm	0.671	0.276	0.371
b = 355 μm	1.163	0.146	0.186
$\epsilon = 11$	2.348	0.088	0.046

TABLE I. Summary of the data presented in Figure 4. For the annular structure the radius of the vacuum channel was $a = 200$ μm and the outer radius was $b = 300$ μm [24].

ture, with beams of varying transverse aspect ratio. For the planar SiO_2 structure, Fig. 3 shows $\bar{x}$ at the downstream BPM as a function of Δx for different normalized beam sizes, χ, and the associated linear fits. As with the annular structure case, the slope of those fit lines is used to calculate the average transverse force per μm offset. It is apparent that for the round beam, $\chi = 0.375$, the measured offset $\bar{x}$ due to transverse forces is greatest for greater initial displacements. As the beam transverse profile is made more elliptical, the transverse wakefield excitation, and thus the observed effect of the initial displacement, is diminished. For the highest aspect ratio beams produced during the experiment, $\chi = 1.875$, the transverse forces are suppressed to near zero, as evidenced by the slope shown in Fig. 3.

The results for the structures and materials available during the experiment, including annular SiO_2, planar SiO_2, and planar Zr-toughened Al_2O_3 (ZTA), are summarized in Table I. These data are shown in Figure 4. The measurement data (circles) agrees well with theoretical calculations (red diamonds). Theoretical values are calculated using the measured experimental beam parameters, with models formulated in Ref. [11] and exact solutions of the Maxwell system for this case from Ref. [10]. Discrepancies between theory and measurements, within the quoted errors, are attributed to deviation in the bunch shape from the theoretically used bi-Gaussian distribution, imperfect alignment of the x and y axes of the beam and the DWA, and the aforementioned transient effects at the entrance and edges.

Figure 4a shows a compilation of the data from the two different planar structures normalized by their respective theoretical maximum values $\bar{F}_{x,max}$. Also shown is the analytical prediction of the χ-scaling given by [11]

$$\frac{\bar{F}_x}{\bar{F}_{x,max}} = \int_{-\infty}^{\infty} dy_0 \frac{e^{\left(-\frac{y_0^2}{2\chi^2}\right)}}{\sqrt{2\pi}\chi} \frac{\left[2-\cosh\left(\frac{\pi}{2}y_0\right)\right]}{\left[\cosh\left(\frac{\pi}{4}y_0\right)\right]^4}. \quad (1)$$

The normalization $\bar{F}_{x,max}$ is calculated using the methods described in Ref.[10] for $\chi = 0$ and with all other beam and structure parameters as described above. Normalization amplitudes $\bar{F}_{x,max}$ were found to be 0.812 MeV/m/μm and 0.738 MeV/m/μm for the SiO_2 and ZTA cases, respectively. After normalization, the comparison shown in Fig. 4a demonstrates the suppression of the transverse wakefield is geometric in origin and not dependent on material type, one of the main predictions of Ref.[11]. Figures 4b and 4c plot the un-normalized data and show reasonable agreement between theory Ref.[10] and experimental results.

Wakefields in beam-driven planar structures have lesser amplitude than those generated in annular structures of equal vacuum apertures [8, 11, 22, 25, 26]. With all other parameters held constant, the ratio of the form factors for transverse wakefields in planar compared to annular structures is $\frac{1}{8}\frac{\pi^4}{16} \approx 0.761$. In these experiments, the form factor comparison is made by dividing the average transverse force $\bar{F}_x$ in the planar structure by $\bar{F}_x$ in the annular case, while accounting for the difference in charges, apertures and χ. The ratio of the form factors is calculated to be 0.8 ± 0.1 and 0.6 ± 0.2 for SiO_2 and ZTA, respectively. The results presented here are in good agreement with the expected value of the form factor ratio.

In conclusion, we have experimentally demonstrated a method for transporting beams in high-gradient wakefield accelerators without commensurately large transverse wakefields. Transverse wakefields are reduced by elliptical shaping of the transverse beam sizes in planar dielectric wakefield accelerators. This approach is separate from methods that rely on external magnetic focusing channels, or those which impose specific longitudinal energy spread correlations in the beams. Comparison of the smallest transverse force to the largest measured in each structure (c.f. Table I) gives a 15-fold reduction in the measured, average transverse forces through elliptical shaping of the beam. These measurements represent a significant step towards efficient, GeV/m wakefield based accelerators, where advanced geometries allow for the design and purposeful control of the modal content for the reduction of beam coupling to undesirable modes [14, 27, 28]. Future work at the forthcoming FACET-II facility will explore effects in advanced structures to demonstrate meter scale, high-gradient acceleration, and permit deeper examination of transverse stability issues.

Work supported by the U.S. Department of Energy under contract numbers DE-AC02-76SF00515 and DE-SC0009914.

* boshea@slac.stanford.edu

[1] B. D. O'Shea *et al.*, Nature Communications **7** (2016).
[2] W. Panofsky and W. Wenzel, Review of Scientific Instru-

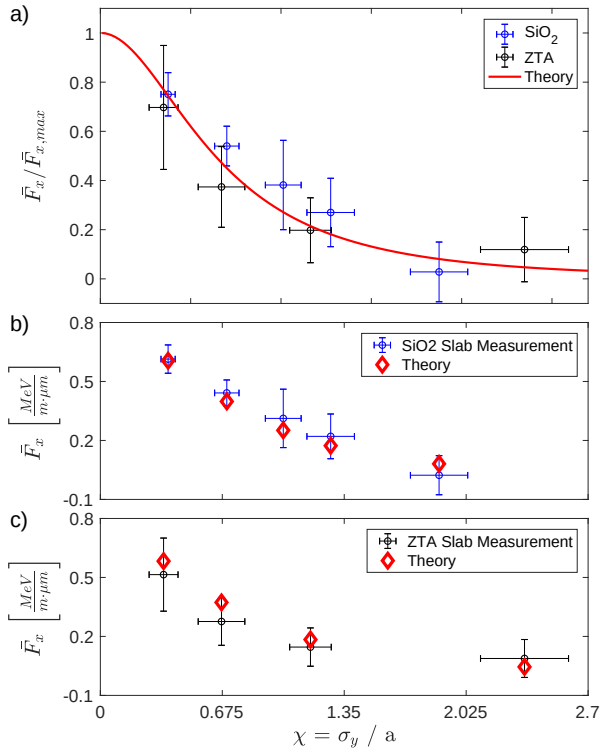

FIG. 4. Panel (a): formula (1) derived in Ref.[11] and normalized experimental values for the average kick SiO_2 (blue) and ZTA (black). Panels (b),(c): The average force per μm offset in the x direction as a function of the normalized beam size, $\chi = \sigma_y/a$, for (b) SiO_2 slabs and (c) ZTA slabs. Parameters for each are contained in Table I. The red diamonds represent theoretical calculations using the methods of Ref.[10] with the parameters described in the text and tables. The blue points represent the measured average force on the beam and the error bars are the 95% confidence intervals.

ments **27**, 967 (1956).

[3] A. W. Chao, *Physics of collective beam instabilities in high energy accelerators* (Wiley, 1993).

[4] S. S. Baturin and A. Zholents, Phys. Rev. Accel. Beams **21**, 031301 (2018).

[5] V. Balakin, A. Novohatsky, and V. Smirnov, Proc. of the 12th Int. Conf. on High Energy Accel. , 119 (1983).

[6] C. Li, W. Gai, J. G. Power, C. X. Tang, and A. Zholents, Phys. Rev. ST Accel. and Beams **17**, 091302 (2014).

[7] A. Zholents, W. Gai, S. Doran, R. Lindberg, J. Power, N. Strelnikov, Y. Sun, E. Trakhtenberg, I. Vasserman, C. Jing, *et al.*, Nuclear Instruments and Methods in Physics Research Section A: Accelerators, Spectrometers, Detectors and Associated Equipment **829**, 190 (2016).

[8] A. Tremaine, J. Rosenzweig, and P. Schoessow, Phys. Rev. E **56** (1997).

[9] D. Mihalcea, P. Piot, and P. Stoltz, Physical Review Special Topics - Accelerators and Beams **15**, 081304 (2012).

[10] S. S. Baturin, I. L. Sheinman, A. M. Altmark, and A. D. Kanareykin, Phys. Rev. ST Accel. Beams **16**, 051302 (2013).

[11] S. S. Baturin, G. Andonian, and J. B. Rosenzweig, Phys. Rev. Accel. Beams **21**, 121302 (2018).

[12] G. Andonian, D. Stratakis, M. Babzien, S. Barber, M. Fedurin, E. Hemsing, K. Kusche, B. O'Shea, X. Wei, O. Williams, V. Yakimenko, and J. B. Rosenzweig, Phys. Rev. Lett. **108**, 244801 (2012).

[13] S. Antipov, C. Jing, A. Kanareykin, J. E. Butler, V. Yakimenko, M. Fedurin, K. Kusche, and W. Gai, Applied Physics Letters **100**, 132910 (2012).

[14] P. D. Hoang, G. Andonian, I. Gadjev, B. Naranjo, Y. Sakai, N. Sudar, O. Williams, M. Fedurin, K. Kusche, C. Swinson, P. Zhang, and J. B. Rosenzweig, Phys. Rev. Lett. **120**, 164801 (2018).

[15] G. Andonian, O. Williams, S. Barber, D. Bruhwiler, P. Favier, M. Fedurin, K. Fitzmorris, A. Fukasawa, P. Hoang, K. Kusche, B. Naranjo, B. O'Shea, P. Stoltz, C. Swinson, A. Valloni, and J. B. Rosenzweig, Phys. Rev. Lett. **113**, 264801 (2014).

[16] M. J. Hogan, T. O. Raubenheimer, A. Seryi, P. Muggli, T. Katsouleas, C. Huang, W. Lu, W. An, K. A. Marsh, W. B. Mori, C. E. Clayton, and C. Joshi, New Journal of Physics **12**, 055030 (2010).

[17] M. Litos, E. Adli, W. An, C. I. Clarke, C. E. Clayton, S. Corde, J. P. Delahaye, R. J. England, A. S. Fisher, J. Frederico, *et al.*, Nature **515**, 92 (2014).

[18] V. Yakimenko, L. Alsberg, E. Bong, G. Bouchard, C. Clarke, C. Emma, S. Green, C. Hast, M. J. Hogan, J. Seabury, N. Lipkowitz, B. O'Shea, D. Storey, G. White, and G. Yocky, Phys. Rev. Accel. Beams **22**, 101301 (2019).

[19] B. D. O'Shea, G. Andonian, S. K. Barber, C. I. Clarke, P. D. Hoang, M. J. Hogan, B. Naranjo, O. B. Williams, V. Yakimenko, and J. B. Rosenzweig, Phys. Rev. Lett. **123**, 134801 (2019).

[20] S. N. Vlasov and I. M. Orlova, Radiophysics and Quantum Electronics **17**, 115 (1974).

[21] S. Antipov *et al.*, Appl. Phys. Lett. **109** (2016).

[22] S. S. Baturin and A. D. Kanareykin, Phys. Rev. Lett. **113**, 214801 (2014).

[23] C. Nieter and J. R. Cary, Journal of Computational Physics **196**, 448 (2004).

[24] A. M. Cook, R. Tikjoplav, S. Y. Tochitsky, G. Travish, O. B. Williams, and J. B. Rosenzweig, Phys. Rev. Lett. **103**, 095003 (2009).

[25] H. Henke and O. Napoly, in *Proceedings of the 2nd European Particle Accelerator Conference, Nice, France, 1990*, European Particle Accelerator Conference (EPAC) (JACoW, Nice, France, 1990) pp. 1046–1048.

[26] K. Bane and G. Stupakov, Nucl. Instrum. Methods Phys. Res., Sect. A **820**, 156 (2016).

[27] C. A. Lindstrøm, E. Adli, J. M. Allen, W. An, C. Beekman, C. I. Clarke, C. E. Clayton, S. Corde, A. Doche, J. Frederico, S. J. Gessner, S. Z. Green, M. J. Hogan, C. Joshi, M. Litos, W. Lu, K. A. Marsh, W. B. Mori, B. D. O'Shea, N. Vafaei-Najafabadi, and V. Yakimenko, Phys. Rev. Lett. **120**, 124802 (2018).

[28] L. Hildebrand, W. An, X. Xu, F. Li, Y. Zhao, M. Hogan, V. Yakimenko, S. Nagaitsev, E. Adli, C. Joshi, *et al.*, in *2018 IEEE Advanced Accelerator Concepts Workshop (AAC)* (IEEE, 2018) pp. 1–5.